Derivation of built-in polarization potentials in nitride-based semiconductor quantum dots

D. P. Williams,[1,*] A. D. Andreev,[2] E. P. O'Reilly,[1] and D. A. Faux[2]
[1]*Tyndall National Institute, Lee Maltings, Prospect Row, Cork, Ireland*
[2]*Advanced Technology Institute, University of Surrey, Guildford GU2 7XH, United Kingdom*
(Received 20 July 2005; revised manuscript received 23 September 2005; published 15 December 2005)

We present a simple analytical approach for the calculation of the built-in strain-induced and spontaneous potentials in nitride-based semiconductor quantum dots. We derive the built-in potentials and electric fields in terms of volume or surface integrals. We describe using a number of simplifying assumptions the general properties of piezoelectric and spontaneous fields in GaN/AlN and InN/GaN quantum dots and obtain analytic solutions to the potential along and close to the axis of symmetry in spherical, cylindrical, cuboidal, truncated-cone, and ellipsoidal dots. We show that the potential distribution in a hexagonal quantum dot is well represented by that of an equivalent dot with circular symmetry. We demonstrate that the built-in electric fields in nitride dots can provide a strong additional lateral confinement for carriers localized in the dot. This additional lateral confinement strongly modifies the electronic structure and optical properties of nitride-based quantum dot structures.

DOI: 10.1103/PhysRevB.72.235318 PACS number(s): 68.65.Hb, 77.65.Ly, 77.22.Ej

I. INTRODUCTION

Nitride-based semiconductor structures have been of considerable interest in recent years.[1,2] Whereas GaAs and most other III–V compounds have a cubic (zinc-blende) crystal structure, GaN and related nitride alloys generally have a hexagonal (wurtzite) structure, which leads to strong built-in fields in quantum wells and heterostructures, of the order of MV/cm. As a consequence, conduction band electrons and valence band holes become spatially separated in GaN-based quantum well structures, with the electron-hole overlap decreasing rapidly for quantum well widths greater than about 50 Å. As well as strong interest in the influence of composition and well-width fluctuations on the electronic structure of InGaN/GaN quantum well structures, there is increasing interest in nitride-based *quantum dot* (QD) structures.[3–5]

A key requirement therefore is for a relatively simple technique to determine the variation in the built-in potential in nitride-based QD structures. There are two contributions to the built-in potential in these systems; the first, referred to as the *spontaneous* potential, arises due to the difference between the QD and matrix materials; the second, referred to as the *strain-induced* or piezoelectric potential, arises due to strain-induced lattice distortions.

We previously presented a Fourier transform method for determining the built-in potential in wurtzite crystals.[6] The method is based on a plane-wave expansion method in which, first, the Fourier transform of the quantum dot characteristic function is calculated explicitly, second, an analytical expression for the built-in potential due to a plane-wave variation in composition is derived, and finally, the built-in potential due to the QD is calculated. The Fourier transform method has demonstrated very clearly that the piezoelectric effect can introduce a strong additional lateral confining potential into a quantum dot, localizing both electrons and holes along the central axis of the dot. However, although this Fourier transform method provides a useful technique for calculating the three-dimensional (3D) built-in potential, it suffers from a number of drawbacks. It does not provide a ready intuitive understanding of how the potential depends on such factors as the dot base-to-height ratio and the relative influence of different contributions to the overall built-in potential. Solutions for an isolated QD, rather than a uniform 3D array, requires a unit cell size large enough for the influence of the surrounding dots to be negligible, which increases the number of Fourier terms required and hence the computation time. Finally, adaptation of the Fourier transform method to dots of unusual shape or variable composition is not easy.

The only alternative method for determining the built-in potential in wurtzite crystals is due to Pan,[7] who determined the Green's functions enabling the piezoelectric potential to be computed for an anisotropic and piezoelectric half-space for a range of surface boundary conditions and accounting for the electromechanical coupling of the piezoelectric potential (but not the spontaneous potential) to the strain. The theory is general, rather complex, and therefore suffers from as many drawbacks as the Fourier transform method. Particularly, it does not provide analytic expressions or simple methods of calculation for the group III-nitride (III-N) system.

It is clearly useful to have a simple real-space technique to determine the built-in potential for the nitride-based semiconductors. Previous authors have presented volume and surface integral expressions for the potential due to the spontaneous polarization of the dot and matrix materials. We extend that work here to present a technique to derive similar volume and surface integral expressions for the strain-induced piezoelectric potential. A number of simplifying assumptions are made in order to make the problem analytically tractable, including isotropic elastic constants and equal elastic, piezoelectric, and dielectric constants in the QD and matrix. We discuss these assumptions in more detail below and how any errors that they introduce should be less than or equal to the error caused by the current uncertainty in the known values of material parameters for nitrides.[8]

The derived surface integral formulas are especially useful for QDs with vertical sides such as cuboidal or cylindrical

dots. Analytical solutions are derived for the built-in potential along and close to the central axis of spherical, cylindrical, cuboidal, truncated-cone, and ellipsoidal dots. The effect of varying the dot shape is investigated, with particular emphasis on the truncated hexagonal pyramid shape, thought to be the actual shape of Stranski-Krastanow grown nitride QDs.[9] The relative contribution of the spontaneous and strain-induced potentials to the total potential is also examined. We show that the potential distribution in a hexagonal quantum dot is very close to that of an equivalent dot with circular symmetry, which can considerably simplify the calculation of energy states in such dots. Overall, the results presented here provide a very useful framework to analyze the built-in potential in nitride-based QDs, providing a simple starting point for more detailed calculations of electron and hole states in such structures.

II. THEORY

The built-in polarization due to quantum dots in wurtzite crystals arises from two sources; that induced by the strain field and that due to the difference in spontaneous polarization between the dot and matrix materials. The piezoelectric polarization induced by a strain field ϵ_{kl} is given by

$$P_i = e_{ijk}\epsilon_{jk}, \tag{1}$$

where e_{ijk} is the tensor of piezoelectric constants. Symmetry considerations allow these 27 constants to be reduced to just three independent components for the wurtzite nitrides (GaN, AlN, InN), which for convenience are renamed: $e_{15} \equiv e_{113}=e_{223}$, $e_{31}\equiv e_{311}=e_{322}$, and $e_{33}\equiv e_{333}$, so that the strain-induced polarization is given by

$$\mathbf{P}_{str} = \begin{pmatrix} 2e_{15}\epsilon_{13} \\ 2e_{15}\epsilon_{23} \\ e_{31}(\epsilon_{11}+\epsilon_{22})+e_{33}\epsilon_{33} \end{pmatrix}. \tag{2}$$

The *spontaneous* polarization arises because the dimensions and atom sites of a III-N unit cell differ slightly from those of an ideal hexagonal crystal. This small deviation introduces spontaneous polarization along the c axis (x_3 direction), $\mathbf{P}_{spo}=P_{spo}\hat{\mathbf{n}}_3$. The total polarization $\mathbf{P}$ is therefore equal to $\mathbf{P}_{str}+\mathbf{P}_{spo}$.

In the theory that follows, a number of simplifying assumptions are made.

(1) It is assumed that the elastic constants of the dot and matrix material are equal. We have argued before that this is a reasonable approximation[10] which can be overcome using iterative techniques.[6]

(2) We have calculated previously the strain due to arrays of dots in crystals of hexagonal symmetry[11,12] but, in order to derive the integral expressions here, the dot and matrix are assumed to have isotropic elastic constants and equal c/a ratios. This should be a reasonable approximation for InN/GaN, where the fractional lattice mismatch along the growth direction (c axis) is similar to that in the lateral direction (a plane; x_1-x_2 plane). It will be a poorer approximation for GaN/AlN, where the lattice mismatch in the lateral and growth directions are different. However, the spontaneous polarization makes the greater contribution to the total potential in GaN/AlN heterostructures, so that any error introduced through the isotropic approximation will be of less overall consequence in this case.

TABLE I. Material parameters of bulk GaN, InN, and AlN used to calculate the piezoelectric fields, from the review article by Vurgaftman and Meyer (Ref. 24), along with derived values. Dielectric constants are from Ref. 13 for GaN and AlN, and Ref. 17 for InN.

Parameter	GaN	AlN	InN
C_{11}, GPa	390	396	223
C_{12}, GPa	145	137	115
C_{13}, GPa	106	108	92
C_{33}, GPa	398	373	224
C_{44}, GPa	105	116	48
a, Å	3.189	3.112	3.545
c, Å	5.185	4.982	5.703
e_{15}, C/m^2	0.33	0.42	0.26
e_{31}, C/m^2	−0.53	−0.54	−0.48
e_{33}, C/m^2	0.89	1.56	1.06
ε_r	9.6	8.5	15
P_{spo}, C/m^2	−0.034	−0.090	−0.042
ν	0.29	0.271	0.353
A	1.82	1.74	2.09
$J\varepsilon_0/\epsilon_0$	0.0057	0.0103	0.0057
$K\varepsilon_0/\epsilon_0$	−0.0091	−0.0107	−0.0056

(3) It is assumed that the piezoelectric constants are independent of material. This is a good approximation for e_{31}, and is also reasonable for e_{15} in the case of GaN/AlN and InN/GaN heterostructures (see Table I). However, it is not so good for e_{33}, particularly in the case of GaN/AlN. We use the piezoelectric constants of the dot material in the calculations below. This minimizes any error in the calculated dot potential due to the difference in e_{33} between the dot and matrix materials.[6,10]

(4) The dielectric constant (relative permittivity) is assumed to be isotropic and independent of material. The argument in favor of this approximation is similar to that for the elastic constants, and can also be corrected using the same iterative techniques.[6,10] Here, we take the isotropic dielectric constant to be $\varepsilon_r=\frac{1}{3}(2\varepsilon_{xx}+\varepsilon_{zz})$, using the *ab initio* values from Ref. 13 for GaN and AlN, giving values of 9.6 for GaN and 8.5 for AlN. The difference between the two is thus less than 12%, in agreement with other studies,[14,15] implying that the approximation is reasonable for GaN/AlN QDs. In the case of InN, the published values vary greatly, from 6.7 (Ref. 16) to 15.3 (Ref. 14), and this uncertainty is compounded by the recent uncertainty in the band gap of InN. We take the most commonly used experimental value, 15, from Ref. 17. The large difference between this value and that of the other nitrides suggests that the approximation must be used with caution for InN/GaN QDs. However, it should still be valid for studies of $In_xGa_{1-x}N$/GaN QDs with moderate values of x, since in this case the dielectric constant of the $In_xGa_{1-x}N$ alloy will be much closer to that of GaN.

(5) It is assumed that the dot is buried within an infinite matrix, thus surface effects are neglected for the matrix. The polarization potential decays over a distance of several dot dimensions,[10] so this is a good approximation provided the dot is not very close to a surface or interface.

(6) It is assumed that the materials are electromechanically uncoupled, that is, the standard isotropic elastic strain solution is used to evaluate the piezoelectric field assuming that the piezoelectric field itself produces a negligible modification of the elastic field. The magnitude of the electromechanical coupling can be estimated by evaluating $g = e_{max}/\sqrt{\varepsilon_{max} C_{max}}$ where e_{max}, ε_{max}, and C_{max} are the maximum values of the piezoelectric constant, dielectric constant, and elastic constant, respectively.[18] A value of g in excess of 0.5 indicates strong coupling, a value of 0.1 or less indicates negligible coupling.[7] InN, GaN, and AlN take values ranging from 0.12 to 0.25, suggesting that electromechanical coupling is small and can safely be neglected. This has been confirmed for InGaN/GaN quantum wells by Christmas *et al.*,[8] where the exact solution for the fully coupled problem is presented and it is shown that the effects of electromagnetic coupling are small. An alternative argument has been provided by Andreev and O'Reilly,[19] where it is shown that the corrections due to electromechanical coupling may be taken into account by renormalizing (or correcting) the material constants and these corrections of the constants are smaller than the uncertainty in their values.

A. Strain-induced piezoelectric potential

We derive here expressions in the form of surface and volume integrals for the electrostatic potential arising from the *strain-induced* polarization in wurtzite crystals. The assumed isotropy of the elastic constants allows Eq. (2) to be modified to

$$\mathbf{P}_{str} = \begin{pmatrix} 2e_{15}\epsilon_{13} \\ 2e_{15}\epsilon_{23} \\ (e_{33}-e_{31})\epsilon_{33} \end{pmatrix} + \frac{2\chi_{QD}\epsilon_0(1-2\nu)e_{31}}{1-\nu}\hat{\mathbf{n}}_3, \tag{3}$$

where we have used the result that, for isotropic systems, the hydrostatic strain, $\epsilon_{11}+\epsilon_{22}+\epsilon_{33}$, is equal to $2\chi_{QD}\epsilon_0(1-2\nu)/(1-\nu)$ (Refs. 20 and 21). ν is Poisson's ratio, equal to $C_{12}/[2(C_{12}+C_{44})]$, C_{ij} are the elastic constants, and C_{11} is constrained to satisfy the isotropic relation $C_{11}-C_{12}-2C_{44}=0$. χ_{QD} is defined as the dot characteristic function, equal to 1 inside the dot and zero outside. Finally ϵ_0 is the isotropic misfit strain, assumed equal to $\frac{1}{3}(2\epsilon_{0a}+\epsilon_{0c})$, where ϵ_{0a} is the misfit strain in the a plane, and ϵ_{0c} is the misfit strain along the c axis.

The strain components can be written as integrals over the surface of the dot[20,22]

$$\epsilon_{ij}(\mathbf{r}) = \delta_{ij}\epsilon_0\chi_{QD} + \frac{\epsilon_0 A}{4\pi}\int_{QD}\frac{(x_i - x_i')}{|\mathbf{r}-\mathbf{r}'|^3}\hat{\mathbf{n}}_j \cdot d\mathbf{S}', \tag{4}$$

where the primed quantities refer to points on the surface of the dot, $(x_1,x_2,x_3)\equiv(x,y,z)$, $\hat{\mathbf{n}}_j$ is the unit vector in the j direction, and $A=(1+\nu)/(1-\nu)$. We can now determine the electrostatic potential using the Maxwell equation $\nabla\cdot\mathbf{D}=0$, where

$$\mathbf{D} = \varepsilon_r\varepsilon_0\mathbf{E} + \mathbf{P} \tag{5}$$

together with the corresponding continuity condition that $\hat{\mathbf{n}}\cdot\mathbf{D}$ must be continuous on crossing the boundary of the dot. Here $\hat{\mathbf{n}}$ is a unit vector normal to the surface of the dot, $\mathbf{D}$ is the electric displacement, ε_r is the relative permittivity, and the electric field, $\mathbf{E}$, is equal to $-\nabla\varphi$, where φ is the electrostatic potential we wish to determine. Thus Eq. (5) becomes

$$\nabla\cdot\mathbf{P}_{str} = \varepsilon_r\varepsilon_0\nabla^2\varphi_{str}. \tag{6}$$

When we substitute Eq. (4) into Eq. (3) for $\mathbf{P}_{str}$, we can then obtain $\nabla\cdot\mathbf{P}_{str}$ and hence $\nabla^2\varphi_{str}$ as the differential of a set of surface integrals. The strain components ϵ_{ij} given by Eq. (4) can be discontinuous on crossing the boundary between the dot and matrix material. We require, however, that $\hat{\mathbf{n}}\cdot\mathbf{D}$ and hence the potential φ_{str} is continuous across the boundary. We use this continuity requirement below to determine φ_{str} for the given strain distribution. In the following derivation, we initially ignore the points on the surface of the dot which give rise to singularities in the integrals of Eq. (4), and hence can take differentials inside or move them outside the integral equations. Substituting Eq. (4) into Eq. (3) for $\mathbf{P}_{str}$ then yields, after a few lines of algebra

$$\begin{aligned}\nabla\cdot\mathbf{P}_{str} = {} & \frac{-2\epsilon_0 A e_{15}}{4\pi}\nabla^2\left\{\int_{QD}\frac{1}{|\mathbf{r}-\mathbf{r}'|}\hat{\mathbf{n}}_3\cdot d\mathbf{S}'\right\} \\ & + \frac{2\epsilon_0 A e_{15}}{4\pi}\frac{\partial^2}{\partial x_3^2}\left\{\int_{QD}\frac{1}{|\mathbf{r}-\mathbf{r}'|}\hat{\mathbf{n}}_3\cdot d\mathbf{S}'\right\} \\ & - \frac{\epsilon_0 A(e_{33}-e_{31})}{4\pi}\frac{\partial^2}{\partial x_3^2}\left\{\int_{QD}\frac{1}{|\mathbf{r}-\mathbf{r}'|}\hat{\mathbf{n}}_3\cdot d\mathbf{S}'\right\}.\end{aligned} \tag{7}$$

Because we ignore for now the points on the dot boundary which give rise to the singularity in the integrands, the first term of Eq. (7) can be taken as equal to zero. It is then easy to show that the final two terms combine to yield

$$\begin{aligned}\nabla\cdot\mathbf{P}_{str} = {} & \left(\frac{-\epsilon_0 A(2e_{15}-e_{33}+e_{31})}{8\pi}\right) \\ & \times\nabla^2\left\{\int_{QD}\frac{(x_3-x_3')^2}{|\mathbf{r}-\mathbf{r}'|^3}\hat{\mathbf{n}}_3\cdot d\mathbf{S}'\right\}.\end{aligned} \tag{8}$$

This result is compared to Eq. (6) whereby is is evident that the strain-induced potential may be written

$$\begin{aligned}\varphi_{str}(\mathbf{r}) &= J\int_{QD}\frac{(x_3-x_3')^2}{|\mathbf{r}-\mathbf{r}'|^3}\hat{\mathbf{n}}_3\cdot d\mathbf{S}' + K\int_{QD}\frac{1}{|\mathbf{r}-\mathbf{r}'|}\hat{\mathbf{n}}_3\cdot d\mathbf{S}' \\ &= JI_1 + KI_2,\end{aligned} \tag{9}$$

where JI_1 may be regarded as a "particular solution" to Eq. (6) and KI_2 as a "constant of integration" for which $\nabla^2 I_2 = 0$ everywhere except on the dot surface. We obtain

$$J = \frac{-\epsilon_0 A(2e_{15} - e_{33} + e_{31})}{8\pi\varepsilon_r\varepsilon_0} \tag{10}$$

from Eq. (8). The value of K is determined by requiring that $\hat{\mathbf{n}}\cdot\mathbf{D}$ and hence φ_{str} be continuous across the boundary. The details of this calculation are presented in Appendix A, giving

$$K = \frac{\epsilon_0}{8\pi\varepsilon_0\varepsilon_r}[4e_{31} + 2e_{33} - A(2e_{15} + e_{31} + e_{33})]. \tag{11}$$

Values of J and K for the nitride-based semiconductors are presented in Table I.

It is noted that Eq. (9) can be confirmed by taking the Fourier transform of Eq. (5), using the known results for the Fourier transform of the strain tensor,[10] and taking the inverse Fourier transform.

Finally, it may be useful in some cases to express φ_{str} in the form of volume integrals. This is easily achieved using Gauss's divergence theorem to obtain

$$\varphi_{str}(\mathbf{r}) = 3J\int_{QD}\frac{(x_3 - x_3')^3}{|\mathbf{r}-\mathbf{r}'|^5}dV' + (K-2J)\int_{QD}\frac{(x_3 - x_3')}{|\mathbf{r}-\mathbf{r}'|^3}dV'. \tag{12}$$

B. Spontaneous potential

The wurtzite crystal structure is hexagonal and, even in an unstrained state, the III-nitride crystal structure deviates slightly from a perfect hexagonal arrangement, resulting in a permanent or spontaneous polarization with the polarization vector pointing along the c axis (x_3 axis).

The potential due to the spontaneous polarization can be derived by using the standard result from electromagnetism for the potential distribution due to a constant polarization field, to obtain,[23]

$$\varphi_{spo}(\mathbf{r}) = \frac{1}{4\pi\varepsilon_r\varepsilon_0}\left[\int_{QD}\frac{\mathbf{P}_{QD}\cdot d\mathbf{S}'}{|\mathbf{r}-\mathbf{r}'|} + \int_M \frac{\mathbf{P}_M\cdot d\mathbf{S}_M}{|\mathbf{r}-\mathbf{r}_M|}\right], \tag{13}$$

where $\mathbf{P}_{QD}$ and $\mathbf{P}_M$ are the constant spontaneous polarizations due to the dot and matrix, respectively. All materials are presumed to have the same relative permittivity. The first integral is taken over the surface of the dot and the second over all surfaces of the matrix (including the outer surface at infinity) and $d\mathbf{S}$ is the usual elemental area with the vector normal to the surface and pointing outwards. The quantity $\mathbf{P}\cdot d\mathbf{S}$ is equivalent to a fictitious charge on a surface element dS. The spontaneous polarization can be rewritten as

$$\varphi_{spo}(\mathbf{r}) = \frac{P_{QD}-P_M}{4\pi\varepsilon_r\varepsilon_0}\int_{QD}\frac{\hat{\mathbf{n}}_3\cdot d\mathbf{S}'}{|\mathbf{r}-\mathbf{r}'|} = \frac{P_{QD}-P_M}{4\pi\varepsilon_r\varepsilon_0}I_2, \tag{14}$$

where we neglect the surface integral taken on the outer surface of the matrix material and the minus sign appears because $d\mathbf{S}'$ is the vector pointing outwards from the surface of the dot. The electrostatic potential φ_{spo} due to the spontaneous polarization difference between the dot and matrix, ΔP_{spo}, is therefore equivalent to the potential due to a charge density $\Delta P_{spo}\hat{\mathbf{n}}_3\cdot\hat{\mathbf{n}}$ distributed over the dot surface.

The electrostatic potential due to the spontaneous polarization difference can also be expressed as a volume integral,

$$\varphi_{spo}(\mathbf{r}) = \frac{P_{QD}-P_M}{4\pi\varepsilon_r\varepsilon_0}\int_{QD}\frac{(x_3 - x_3')}{|\mathbf{r}-\mathbf{r}'|^3}dV'. \tag{15}$$

Equations (9), (12), (14), and (15) are key results of the paper, enabling the strain-induced and spontaneous potentials to be determined by evaluating surface or volume integrals for a wurtzite material within the isotropic approximation. The surface integral is especially useful for QDs with surfaces parallel to the x_3 axis, such as the cylinder or cuboid, where the integrals are nonzero only for those surfaces perpendicular to the x_3 axis.

C. Special solutions

Results may be generated by evaluating explicitly the integrals derived in the previous sections. For example, the electric field due to the spontaneous potential may be evaluated from $\mathbf{E}_{spo} = -\nabla\varphi_{spo}$ using Eq. (14). This yields

$$\mathbf{E}_{spo} = \frac{P_{QD}-P_M}{4\pi\varepsilon_r\varepsilon_0}\int_{S'}\frac{(x_i - x_i')\hat{\mathbf{n}}_i}{|\mathbf{r}-\mathbf{r}'|^3}\hat{\mathbf{n}}_3\cdot d\mathbf{S}', \tag{16}$$

where the usual summation convention is used for repeated indices. It is interesting to note that the spontaneous electric field components $E_{k,spo}$ have the same functional form as the *relaxation* strain components ϵ^r_{k3}, with the integral to determine $E_{k,spo}$ in Eq. (16) being identical to the integral determining ϵ^r_{k3} in Eq. (4). [The relaxation strain, ϵ^r_{ij}, is equivalent to the second term in Eq. (4), i.e., it is the strain not including the initial misfit strain.[22]] Similarly, the strain-induced electric field is obtained from Eq. (9) as

$$\mathbf{E}_{str} = 3J\int_{S'}\frac{(x_i - x_i')(x_3 - x_3')^2\hat{\mathbf{n}}_i}{|\mathbf{r}-\mathbf{r}'|^5}\hat{\mathbf{n}}_3\cdot d\mathbf{S}' + (K - \delta_{i3}2J)\int_{S'}\frac{(x_i - x_i')\hat{\mathbf{n}}_i}{|\mathbf{r}-\mathbf{r}'|^3}\hat{\mathbf{n}}_3\cdot d\mathbf{S}'. \tag{17}$$

There are several important cases where we can use the equations derived to obtain analytical solutions for the built-in potential in a nitride-based QD, in particular along and close to the central x_3 axis. These solutions are particularly useful, since the electron and hole wave functions are generally centered on this high-symmetry axis.[6] The integrals I_1 and I_2 can be solved analytically along the central x_3 axis for any regular n-gon-shaped surface, oriented in the x_1-x_2 plane (see Appendix B). This immediately provides the potential along the central axis for any dot with a regular cross section and vertical sides. A complete analytical solution can be obtained for the built-in potential due to a cubic dot, as well as solutions for the potential, $\varphi_0(z) = \varphi(0,0,x_3)$, along the $\hat{\mathbf{n}}_3$ axis for spherical, cylindrical, truncated cone, ellipsoidal, and spherical cap dot shapes. These are presented in Appendix B.

We also include in Appendix B expressions for $\partial_x^2\varphi$ at $x = y = 0$ as a function of z, (where $\partial_i\varphi$ is the partial derivative

of φ with respect to the variable i), which can be used to obtain an approximation for the lateral variation of the potential close to the $\hat{\mathbf{n}}_3$ axis. The expression

$$\varphi(x_1,x_3) = \varphi(x,z) = \varphi_0(z) + \frac{1}{2}x^2\partial_x^2\varphi(z) \tag{18}$$

gives less than 1% error out to about half the radius of the dot, when compared to the numerically calculated potential. This then gives a useful analytical approximation for the total potential over the most important region of the dot.

The expression for the lateral potential variation is easy to obtain for the spontaneous potential. We note that $\nabla\cdot\mathbf{E}_{spo}=0$ and that for the cases presented here the potential has circular symmetry close to $x=y=0$. This implies that

$$\partial_x^2\varphi_{spo} = -\frac{1}{2}\partial_z^2\varphi_{spo} \tag{19}$$

so that $\partial_x^2\varphi$ can then be obtained immediately from the second derivative $\partial_z^2\varphi(z)$ along the z axis. This result also holds for the second term, I_2, of the strain-induced potential. We evaluate $\partial_x^2 I_1$ directly, giving

$$\partial_x^2 I_1 = 15\int_{QD}\frac{(x_1-x_1')^2(x_3-x_3')^2}{|\mathbf{r}-\mathbf{r}'|^7}\hat{\mathbf{n}}_3\cdot d\mathbf{S}' - 3\int_{QD}\frac{(x_3-x_3')^2}{|\mathbf{r}-\mathbf{r}'|^5}\hat{\mathbf{n}}_3\cdot d\mathbf{S}'. \tag{20}$$

Equations (19) and (20) are then used to obtain the expressions for the lateral variation of the potential presented in Appendix B.

III. ANALYSIS OF GaN/AlN AND InN/GaN QUANTUM DOTS

We now use this surface integral method to investigate the built-in potential in GaN/AlN and InN/GaN quantum dots. The material parameters used are taken from Vurgaftman and Meyer[24] (see Table I). We use the dot material values for ε_r and the e_{ij} throughout, and the matrix value for ν, as in Refs. 6 and 10. For nitrides, the lattice mismatch is different in the c direction than in the a direction, hence the misfit strain has a value ϵ_{0c} in the z direction and a different value ϵ_{0a} in the x and y directions. For the isotropic approximation, we use a three-dimensional average of this, taking $\epsilon_0=(2\epsilon_{0a}+\epsilon_{0c})/3$. We begin by comparing the potentials due to the interface between square and circular GaN planes and an AlN matrix. In practice, the full potential in a cylindrical or cuboidal QD of height h will involve taking the difference between the potentials due to two such interfaces a distance h apart. We focus here for illustrative purposes on the potential due to one of the interfaces.

Figure 1 shows the potential in the x-y plane at $z=0$ for a square plane of side 10 nm and a circular plane of radius $10/\sqrt{\pi}$ nm—the dimensions are chosen so that the two planes have equal area. The plots are divided along the line for which the radius of the circle is the same as for the cross section of the square, demonstrating that the contours along this line are almost identical for the two shapes. Both surfaces exhibit a large potential well in the center, which will contribute to the lateral carrier confinement in the dot. Notice that the magnitude of this potential can reach 2.85 V which is comparable to band-gap potentials, emphasizing that built-in potentials must be accounted for in calculations involving nitrides. The square geometry introduces only slight variations to the circular distribution, which rapidly become less noticeable on moving away from the dot. Figure 2 shows the potential along the central z axis as a function of distance z from the square and circular planes of Fig. 1. It can be seen that the potential along this axis due to the two planes is almost identical, with at most a 0.55% difference between the two.

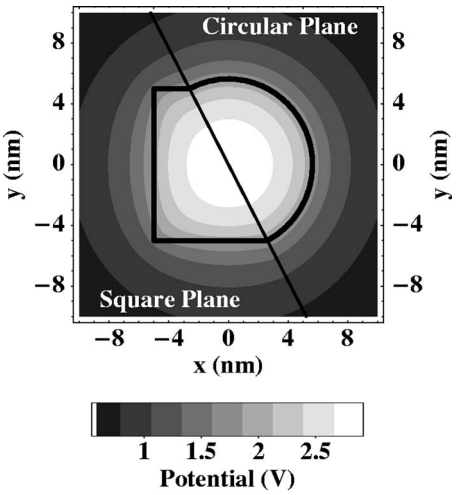

FIG. 1. Contour plot showing the built-in potential in the x-y plane at $z=0$ due to a square and a circular GaN/AlN planar interface.

Experimental studies indicate that real nitride quantum dots have a truncated hexagonal pyramid shape,[9] for which the potential needs to be calculated numerically. However, the discussion above suggests that the potential within a truncated hexagonal pyramid dot should be well approximated

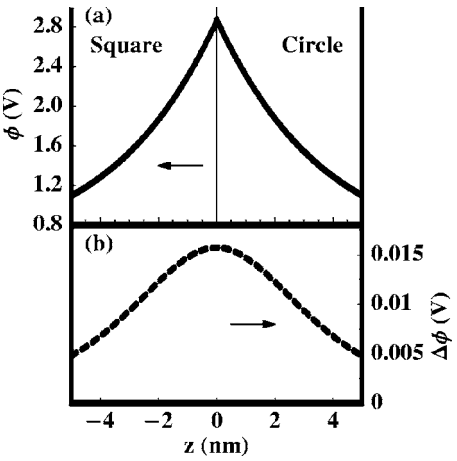

FIG. 2. (a) Built-in potential along the central z axis due to a square ($z<0$) and a circular ($z>0$) GaN/AlN planar interface and (b) the difference between the two, $\Delta\varphi=\varphi_{Circ}-\varphi_{Sqr}$ (for all z).

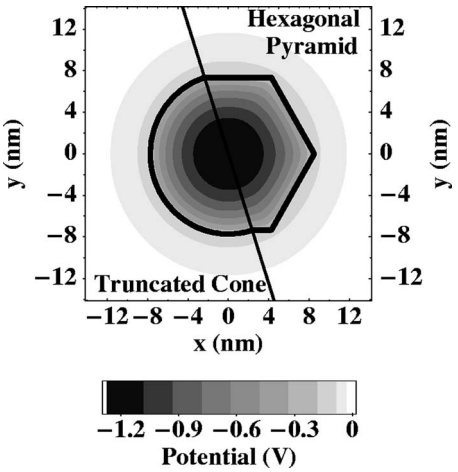

FIG. 3. Contour plot in the *x*-*y* plane for a GaN/AlN truncated cone dot and a truncated hexagonal pyramid dot.

by that of a truncated cone dot of the same volume and shape. Use of this approximation reduces the potential variation to a function of two variables (r,z) rather than three, thereby simplifying the solution of Schrödinger's equation. The surface integrals I_1 and I_2 for a truncated cone can also be partially solved analytically (in terms of elliptic functions), greatly reducing the computation time required to determine the built-in potential. With this in mind, Fig. 3 compares the total built-in potential in the *x*-*y* plane at $z=0$ for a truncated cone and a truncated hexagonal pyramid with the same height, side angle, and volume. Again, the plot is divided along the line of equal radii. Figure 4 plots the potential in the *r*-*z* plane taken along this line, while Fig. 5 shows the potential variation along the central *z* axis of the two structures. There is excellent quantitative agreement between the two potentials, with the maximum difference in potential along the *z* axis of the order of 1.5 mV, an order of magnitude smaller than the difference between the square and circular results in Figs. 1 and 2.

Figures 3–5 also illustrate some typical properties of the built-in potential in nitride QDs. There is a large potential difference between the top and bottom of the dot, which leads to a spatial separation of confined electrons and holes, since the electrons will be attracted towards the top of the dot, while the holes are attracted towards the bottom of the dot. This results in a built-in dipole moment and a redshift of exciton emission energies with respect to the band-gap

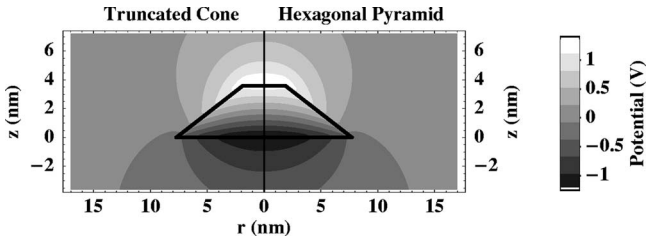

FIG. 4. Contour plot in the *r*-*z* plane comparing the built-in potential of a GaN/AlN truncated cone dot (left) and a truncated hexagonal pyramid dot (right) of equal volumes, taken along the line of equal radii.

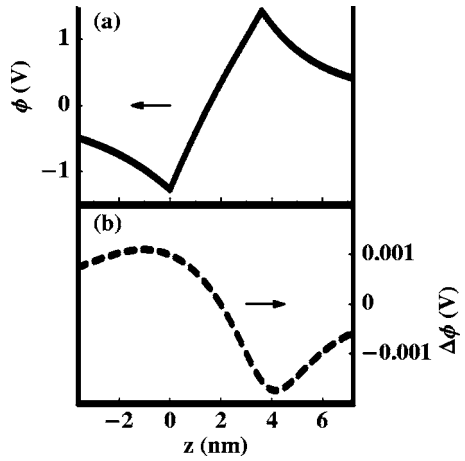

FIG. 5. (a) Built-in potential along the central *z* axis for a GaN/AlN truncated cone and a truncated hexagonal pyramid (indistinguishable in this plot) and (b) the difference between the two, $\Delta\varphi=\varphi_{Pyr}-\varphi_{Cone}$.

energy.[3,25] The built-in potential also provides an additional lateral confinement for both electrons and holes, ensuring they are well-confined within the dot, close to the central axis.

The results presented in Figs. 3–5 were for GaN/AlN quantum dot structures. We find that similar conclusions are also obtained when we consider InN/GaN systems. The relative contribution of the spontaneous and strain-induced potentials to the total potential depends on the dot and matrix compositions. For GaN/AlN, the spontaneous and strain-induced potentials contribute approximately equally, while in InN/GaN, the potential is almost entirely strain-induced (Fig. 6). The weak spontaneous potential in InN/GaN is due to the small difference in the spontaneous polarization constants of the two materials, about a factor of 7 smaller than in GaN/AlN. However, the decrease in the total potential for an InN/GaN QD compared to an equivalent GaN/AlN QD is less than might be expected, due to an increase in the strain-induced contribution. This is principally caused by the larger lattice mismatch in InN/GaN, which results in a greater magnitude of the misfit strain ϵ_0. (This is slightly offset by an increase in the relative permittivity, ε_r.) There is increasing interest in $In_xGa_{1-x}N/GaN$ quantum dot structures, grown by a variety of methods.[26,27] Considerable uncertainty still remains concerning the structure of these dots, including dot composition and whether the composition is constant or varies through the dot. Uncertainty also persists concerning some of the material parameters for nitrides, especially InN

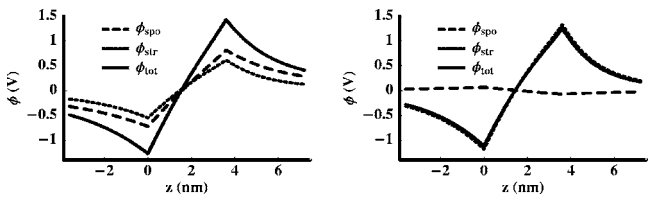

FIG. 6. Spontaneous and strain-induced contributions to the total built-in potential for a GaN/AlN QD (left) and an InN/GaN QD (right).

and by extension $In_xGa_{1-x}N$. The sensitivity of calculated dot properties to material parameters can present difficulties in experimental analysis. We suggest, however, that if the geometry of a dot is accurately known from structural measurements, then the surface or volume integral methods presented here may prove useful in combination with other techniques to refine the values of some of these parameters.[28]

IV. CONCLUSION

We have presented in this paper a straightforward method for determining the built-in potential, both spontaneous and strain-induced, due to a quantum dot in an isotropic nitride-like system. The technique involves evaluating two integrals, either over the surface of the dot [Eqs. (9) and (14)] or equivalently over the volume of the dot [Eqs. (12) and (15)]. Unlike other methods used, it has the advantage that it is an entirely real-space technique, thus providing a more intuitive understanding of the factors which influence the built-in potential, as well as admitting analytical solutions in certain cases. We have calculated the full analytical solution for the built-in potential in a cubic dot, and analytical solutions for the potential along the central x_3 axis for spherical, cylindrical, truncated cone, ellipsoidal, and spherical cap dot shapes. Moreover, we have shown how it is possible to obtain an analytical approximation for the lateral variation of the potential close to the x_3 axis, thus providing a full analytical expression for the potential in the region of the central axis, where electron and hole wave functions are expected to be large.

We have demonstrated that the potential due to a circular surface is remarkably similar to that due to a square surface of equal area, with even closer agreement obtained between a hexagonal and circular surface. This allows, in theoretical studies, the replacement of a truncated hexagonal pyramid shape, which is the most likely shape for actual nitride dots, with a truncated cone shape of the same volume. Such an approximation introduces only minor errors in the built-in potential, and can considerably simplify the solution of the Schrödinger equation.

Finally, we have reviewed the contributions of the strain-induced and spontaneous potentials to the total built-in potential. We have shown that in GaN/AlN systems the two contribute a similar amount to the total potential, while in InN/GaN the spontaneous contribution is very small due to the much smaller difference in polarization constants, and so the potential is almost entirely strain-induced. In both cases, the piezopotential produces large electric fields along the growth direction, spatially separating confined electrons and holes. The potential also provides an additional lateral confinement within the dot. In conclusion, the technique presented here provides a very useful method to calculate the built-in potential due to an arbitrarily shaped nitride quantum dot, of considerable value for theoretical studies of such systems.

ACKNOWLEDGMENTS

We thank G. S. Pearson for useful contributions, Science Foundation Ireland, and the Irish Research Council for Science, Engineering and Technology (DPW) for financial support.

APPENDIX A

The value of K is determined from the condition that $\hat{\mathbf{n}}\cdot\mathbf{D}$ must be continuous across the boundary. For our purposes, it is sufficient to consider the case where $\hat{\mathbf{n}}=\hat{\mathbf{n}}_3$, noting that any closed surface will have at least one point where this is the case. This gives

$$\hat{\mathbf{n}}_3\cdot\mathbf{D} = -\varepsilon_r\varepsilon_0\left((2J-K)\int_{QD}\frac{(x_3-x_3')}{|\mathbf{r}-\mathbf{r}'|^3}\hat{\mathbf{n}}_3\cdot d\mathbf{S}' - 3J\int_{QD}\frac{(x_3-x_3')^3}{|\mathbf{r}-\mathbf{r}'|^5}\hat{\mathbf{n}}_3\cdot d\mathbf{S}'\right) + (e_{33}-e_{31})\frac{\epsilon_0 A}{4\pi}\int_{QD}\frac{(x_3-x_3')}{|\mathbf{r}-\mathbf{r}'|^3}\hat{\mathbf{n}}_3\cdot d\mathbf{S}'$$
$$+ (e_{33}-e_{31})\epsilon_0\chi_{QD} + \frac{2(1-2\nu)}{(1-\nu)}\epsilon_0 e_{31}\chi_{QD}. \tag{A1}$$

Each of the integrals in Eq. (A1) has a step discontinuity at the boundary of the quantum dot. To determine the magnitude of this step at the point where $\hat{\mathbf{n}}=\hat{\mathbf{n}}_3$, consider the region around this point with dimensions small enough that the dot surface can be considered planar over the region. Now, construct a cylinder with its top surface on the surface of the QD, of radius R and height $2h$ sufficiently small that the entire cylinder is contained within the dot (Fig. 7).

The step change at the top surface of this cylinder will then be the same as the step change for the whole dot (at this point). Integrating over the cylinder, the side surfaces make no contribution since $\hat{\mathbf{n}}_3\cdot d\mathbf{S}'=0$ here, and so, with $\mathbf{r}$ on the central axis of the cylinder, the first integral in Eq. (A1) becomes

$$\int_0^R\int_0^{2\pi}\frac{(z-h)r}{(r^2+(z-h)^2)^{3/2}}d\theta dr - \int_0^R\int_0^{2\pi}\frac{(z+h)r}{(r^2+(z+h)^2)^{3/2}}d\theta dr. \tag{A2}$$

Now, using the substitution $u^2=r^2+(z\pm h)^2$, or otherwise, the solution is found to be

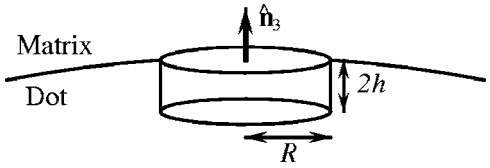

FIG. 7. Surface over which the integration is performed.

$$= 2\pi[\mathrm{sgn}(z-h) - \mathrm{sgn}(z+h)] - 2\pi\left(\frac{z-h}{\sqrt{R^2+(z-h)^2}} - \frac{z+h}{\sqrt{R^2+(z+h)^2}}\right) \quad \text{(A3)}$$

where $\mathrm{sgn}(x)=1$ if $x>0$, 0 if $x=0$, and -1 if $x<0$. These sgn terms can be rewritten as $\mathrm{sgn}(z-h)-\mathrm{sgn}(z+h)\equiv -2\chi_{Cyl}$, where χ_{Cyl} is the characteristic function of the cylinder. Now, considering the two cases $z\to h$ from above (where it is outside the dot at all times) and $z\to h$ from below (where it is inside the dot at all times), it can be seen that there is a difference of 4π between the two limits, resulting in a step of -4π on going from outside to inside the dot. Similarly, it can be shown that there is a corresponding step change of $-4\pi/3$ for the second integral in Eq. (A1). It is now a simple matter to substitute these results into Eq. (A1) to find

$$K = \frac{\epsilon_0}{8\pi\varepsilon_0\varepsilon_r}[4e_{31}+2e_{33}-A(2e_{15}+e_{31}+e_{33})] \quad \text{(A4)}$$

APPENDIX B

1. Full analytical solution for a cubic dot

For a cubic dot centered at the origin, with width $2B_x$, depth $2B_y$, and height $2h$, we derive that

$$I_1(x,y,z) = J_1(x,y,z-h) - J_1(x,y,z+h), \quad \text{(B1)}$$

$$I_2(x,y,z) = J_2(x,y,z-h) - J_2(x,y,z+h), \quad \text{(B2)}$$

$$J_1(x,y,z) = z\,\mathrm{sgn}(z)\sum_{\xi,\eta}\sin^{-1}\left(\frac{\xi_\pm\eta_\pm}{\sqrt{\xi_\pm^2+z^2}\sqrt{\eta_\pm^2+z^2}}\right), \quad \text{(B3)}$$

$$J_2(x,y,z) = \sum_{\xi,\eta}\left[\xi_\pm\sinh^{-1}\left(\frac{\eta_\pm}{\sqrt{\xi_\pm^2+z^2}}\right) + \eta_\pm\sinh^{-1}\left(\frac{\xi_\pm}{\sqrt{\eta_\pm^2+z^2}}\right)\right] - J_1(x,y,z), \quad \text{(B4)}$$

where $\xi_\pm = B_x \pm x$, $\eta_\pm = B_y \pm y$, and $\mathrm{sgn}(x)=1$ if $x>0$, 0 if $x=0$, and -1 if $x<0$. For each sum, the expression is evaluated twice, the first time using the plus sign in the indicated variable, and the second time using the minus sign. So, for example, $\Sigma_\xi(\xi_\pm)=\xi_+ + \xi_-$ and $\Sigma_{\xi,\eta}(\xi_\pm\eta_\pm)=\xi_+\eta_+ + \xi_+\eta_- + \xi_-\eta_+ + \xi_-\eta_-$.

2. Analytical expressions along z axis

(a) Regular n-gon plane, centered at origin, with D the perpendicular distance to the n-gon side;

$$I_1 = 2\pi z\,\mathrm{sgn}(z) - 2nz\sin^{-1}\left(\frac{z\sin\left(\frac{\pi}{n}\right)}{\sqrt{D^2+z^2}}\right), \quad \text{(B5)}$$

$$I_2 = 2nD\sinh^{-1}\left(\frac{D\tan\left(\frac{\pi}{n}\right)}{\sqrt{D^2+z^2}}\right) - I_1. \quad \text{(B6)}$$

(b) Sphere, centered at origin, radius a;

$$I_1 = \frac{2\pi}{3z^4}\,\mathrm{sgn}(z\pm a)\left(-\frac{6}{5}a^5 + a^3z^2 \pm \frac{z^5}{5}\right), \quad \text{(B7)}$$

$$I_2 = \frac{2\pi}{3z^2}\,\mathrm{sgn}(z\pm a)(a^3 \pm z^3). \quad \text{(B8)}$$

(c) Cylinder, centered at origin, radius a, height $2h$;

$$I_1 = \pm 2\pi\left(\frac{(z\pm h)^2}{\sqrt{a^2+(z\pm h)^2}} - (z\pm h)\mathrm{sgn}(z\pm h)\right), \quad \text{(B9)}$$

$$I_2 = \pm 2\pi(-\sqrt{a^2+(z\pm h)^2} + (z\pm h)\mathrm{sgn}(z\pm h)). \quad \text{(B10)}$$

(d) Truncated cone, with its base centered on the origin, base radius R_b, top radius R_t. The truncation factor f is given by $f=(1-R_t/R_b)$ and the height of the dot is then given by hf, where h is the height of the untruncated cone. We also define the angle $\phi=\sin^{-1}(R_b/\sqrt{R_b^2+h^2})$, which is half the opening angle of the cone, and let

$$\lambda_b = \sqrt{R_b^2+z^2}, \quad \lambda_t = \sqrt{R_t^2+(z-hf)^2}$$

$$\alpha_b = R_b\sin(\phi) + z\cos(\phi) + \lambda_b,$$

$$\alpha_t = R_t\sin(\phi) + (z-hf)\cos(\phi) + \lambda_t,$$

$$I_1 = 2\pi\Bigg\{-z\,\mathrm{sgn}(z) + (z-hf)\mathrm{sgn}(z-hf) + \frac{z}{\lambda_b}[z\cos^2(\phi) - h\sin^2(\phi)] - \frac{z-hf}{\lambda_t}[(z-hf)\cos^2(\phi) - (h-hf)\sin^2(\phi)] + \sin^2(\phi)\cos(\phi)\Bigg[3(\lambda_b-\lambda_t)\cos(\phi) + (h-z)[1-3\sin^2(\phi)]\ln\left(\frac{\alpha_b}{\alpha_t}\right)\Bigg]\Bigg\}, \quad \text{(B11)}$$

$$I_2 = 2\pi\Bigg\{z\,\mathrm{sgn}(z) - (z-hf)\mathrm{sgn}(z-hf) - \lambda_b\cos^2(\phi) + \lambda_t\cos^2(\phi) + (h-z)\cos(\phi)\sin^2(\phi)\ln\left(\frac{\alpha_b}{\alpha_t}\right)\Bigg\}. \quad \text{(B12)}$$

(e) Ellipsoid, centered at the origin, with axis of symmetry in the z direction, semimajor radius a (in the x-y plane), and semiminor radius b (in the z-plane), with $c^2=a^2-b^2$.

$$I_1 = 2\pi\left\{\frac{a^2b(2a^2+b^2)z}{c^5}\sin^{-1}\left(\frac{a-\frac{b}{a}(z\pm b)}{\sqrt{c^2+z^2}}\right)\right\}, \quad \text{(B13)}$$

$$I_2 = \pm\frac{2\pi a^2}{c^2}(z\pm b)\mathrm{sgn}(z\pm b) - \frac{2\pi a^2bz}{c^3}\sin^{-1}\left(\frac{a-\frac{b}{a}(z\pm b)}{\sqrt{c^2+z^2}}\right). \quad \text{(B14)}$$

(f) Spherical cap, with its base centered at the origin, base radius a, height h. The radius of the underlying sphere is $\rho = 1/2h(a^2+h^2)$ and $f=\rho-h$, $\xi=z+f$.

$$I_1 = 2\pi\left\{-\frac{(a^2+z^2)^{5/2}}{15\xi^4} + \frac{(2\rho^2+3f^2+2f\xi)(a^2+z^2)^{3/2}}{3\xi^4} - \frac{[\rho^2(\rho^2+f^2)-2f^3\xi]\sqrt{a^2+z^2}}{\xi^4} + \frac{z^3}{\xi\sqrt{a^2+z^2}} - \frac{1}{15\xi^4}(6\rho^5-5\rho^3\xi^2-\xi^5)\mathrm{sgn}(z-h) - z\,\mathrm{sgn}(z)\right\} \quad \text{(B15)}$$

$$I_2 = \frac{2\pi}{3}\left\{\sqrt{a^2+z^2}\left(\frac{\rho^2-z\xi}{\xi^2}-1\right) - \left(\frac{\xi^3-\rho^3}{\xi^2}\right)\mathrm{sgn}(z-h)\right\} + 2\pi z\,\mathrm{sgn}(z) \quad \text{(B16)}$$

3. $\partial_x^2\varphi$ along z axis

(a) Spherical QD, centered at origin, with radius a;

$$\partial_x^2\varphi_{sph}(z) = \pm\mathrm{sgn}(a\pm z)\frac{2\pi a^3}{z^4}\left\{\frac{J}{z^2}(4a^2-3z^2) - K - \frac{P_{QD}-P_M}{4\pi\varepsilon_r\varepsilon_0}\right\} \quad \text{(B17)}$$

(b) Cylindrical QD, radius a, height $2h$, centered on the origin;

$$\partial_x^2\varphi_{Cyl}(z) = 3\pi a^2 J\left(\pm\frac{(z\pm h)^2}{[a^2+(z\pm h)^2]^{5/2}}\right) + \pi a^2\left(K+\frac{P_{QD}-P_M}{4\pi\varepsilon_r\varepsilon_0}\right)\left(\pm\frac{1}{[a^2+(z\pm h)^2]^{3/2}}\right) \quad \text{(B18)}$$

(c) Cuboidal QD, dimensions $2a\times2b\times2c$, centered on the origin. Let $d=\sqrt{a^2+b^2+(z\pm c)^2}$;

$$\partial_x^2\varphi_{cub}(z) = 4Jab\left(\pm\frac{(z\pm c)^2(3d^2-b^2)}{(d^2-b^2)^2d^3}\right) + 4ab\left(K+\frac{P_{QD}-P_M}{4\pi\varepsilon_r\varepsilon_0}\right)\left(\pm\frac{1}{(d^2-b^2)d}\right) \quad \text{(B19)}$$

(d) Conical QD, base radius a, height h truncated by a fraction f. The base is centered on the origin and the axis of symmetry is along the z direction;

$$\partial_x^2\varphi_{con}(z) = \pi\left(\frac{h}{h-z}\right)\left\{3J\left(\frac{a^2z^2}{(a^2+z^2)^{5/2}} - \frac{a^2(1-f)^3(z-hf)^2}{[a^2(1-f)^2+(z-hf)^2]^{5/2}}\right) + \left(K+\frac{P_{QD}-P_M}{4\pi\varepsilon_r\varepsilon_0}\right)\times\left(\frac{a^2}{(a^2+z^2)^{3/2}} - \frac{a^2(1-f)^3}{[a^2(1-f)^2+(z-hf)^2]^{3/2}}\right)\right\}. \quad \text{(B20)}$$

(e) Ellipsoid, centered at the origin, with axis of symmetry in the z direction, semimajor radius a (in the x-y plane), and semiminor radius b (in the z plane), with $c^2=a^2-b^2$

$$\partial_x^2\varphi_{ell}(z) = [\pm\mathrm{sgn}(a\pm z)]\frac{2\pi a^2b}{(a^2-b^2+z^2)^2}\times\left\{J\left(\frac{a^2+3(b^2-z^2)}{a^2-b^2+z^2}\right) - \left(K+\frac{P_{QD}-P_M}{4\pi\varepsilon_r\varepsilon_0}\right)\right\}. \quad \text{(B21)}$$

(f) Spherical cap, with its base centered at the origin, base radius a, height h. The radius of the underlying sphere is $\rho = 1/2h(a^2+h^2)$ and $f=\rho-h$, $\xi=z+f$.

$$\partial_x^2\varphi_{sc}(z) = \pi J\left(\frac{2\rho^3(4\rho^2-3\xi^2)}{\xi^6}\,\mathrm{sgn}(h-z) + \frac{3z^2a^2}{(a^2+z^2)^{5/2}} - \frac{3(\rho^2-\xi^2)^4(\rho^2+\xi^2)}{32\xi^6(a^2+z^2)^{5/2}} + \frac{(\rho^2-\xi^2)^2(25\rho^4+2\rho^2\xi^2-3\xi^4)}{32\xi^6(a^2+z^2)^{3/2}} - \frac{3(\rho^2-\xi^2)[24\rho^4+(\rho^2-\xi^2)^2]}{16\xi^6\sqrt{a^2+z^2}} - \frac{64\rho^4-3f\xi^2(3z+f)-\rho^2\xi(44z+25f)}{16\xi^6}\sqrt{a^2+z^2}\right) + \pi\left(K+\frac{P_{QD}-P_M}{4\pi\varepsilon_r\varepsilon_0}\right)\left(-\frac{2\rho^3}{\xi^4}\,\mathrm{sgn}(h-z) + \frac{2\rho^4+z\xi a^2}{\xi^4\sqrt{a^2+z^2}} - \frac{f(a^2[a^2-z^2+(z-f)^2]+2f^2z^2)}{\xi^3(a^2+z^2)^{3/2}} - \frac{a^2}{(a^2+z^2)^{3/2}}\right). \quad \text{(B22)}$$

*Email address: williams@tyndall.ie

[1] S. C. Jain, M. Willander, J. Narayan, and R. Van Overstraeten, J. Appl. Phys. **87**, 965 (2000).
[2] *Group III Nitride Semiconductor Compounds: Physics and Applications*, edited by B. Gil (Clarendon Press, Oxford, UK, 1998).
[3] F. Widmann, J. Simon, B. Daudin, G. Feuillet, J. L. Rouvière, N. T. Pelekanos, and G. Fishman, Phys. Rev. B **58**, R15989 (1998).
[4] S. Ruffenach, B. Maleyre, O. Briot, and B. Gil, Phys. Status Solidi C **2**, 826 (2005).
[5] V. Ranjan, G. Allan, C. Priester, and C. Delerue, Phys. Rev. B **68**, 115305 (2003).
[6] A. D. Andreev and E. P. O'Reilly, Phys. Rev. B **62**, 15851 (2000).
[7] E. Pan, Proc. R. Soc. London, Ser. A **458**, 181 (2002).
[8] U. M. E. Christmas, A. D. Andreev, and D. A. Faux, J. Appl. Phys. **98**, 073522 (2005).
[9] M. Arley, J. L. Rouvière, F. Widmann, B. Daudin, G. Feuillet, and H. Mariette, Appl. Phys. Lett. **74**, 3287 (1999).
[10] A. D. Andreev, J. R. Downes, D. A. Faux, and E. P. O'Reilly, J. Appl. Phys. **86**, 297 (1999).
[11] A. D. Andreev and E. P. O'Reilly, MRS Internet J. Nitride Semicond. Res. **4S1**, G6.45 (1999).
[12] A. D. Andreev and E. P. O'Reilly, Thin Solid Films **364**, 291 (2000).
[13] J.-M. Wagner and F. Bechstedt, Phys. Rev. B **66**, 115202 (2002).
[14] H. Harima, J. Phys.: Condens. Matter **14**, R967 (2002).
[15] J. A. Chisholm, D. W. Lewis, and P. D. Bristowe, J. Phys.: Condens. Matter **11**, L235 (1999).
[16] C. Persson, R. Ahuja, A. Ferreira da Silva, and B. Johansson, J. Phys.: Condens. Matter **13**, 8945 (2001).
[17] *Properties of Group-III Nitrides*, EMIS Datareviews Series, edited by J. H. Edgar (INSPEC, London, 1994).
[18] Z. Suo, C.-M. Kuo, D. M. Barnett, and J. R. Willis, J. Mech. Phys. Solids **40**, 739 (1992).
[19] A. D. Andreev and E. P. O'Reilly, Nanotechnology **11**, 256 (2000).
[20] J. R. Downes, D. A. Faux, and E. P. O'Reilly, J. Appl. Phys. **81**, 6700 (1997).
[21] D. Bimberg, M. Grundmann, and N. N. Ledentsov, *Quantum Dot Heterostructures* (Wiley, Chichecster, UK, 1998).
[22] J. H. Davies, J. Appl. Phys. **84**, 1358 (1998).
[23] C. Kittel, *Introduction to Solid State Physics*, 7th ed. (Wiley, Chichester, UK, 1995).
[24] I. Vurgaftman and J. R. Meyer, J. Appl. Phys. **94**, 3675 (2003).
[25] D. P. Williams, A. D. Andreev, and E. P. O'Reilly, Superlattices Microstruct. **36**, 791 (2004).
[26] K. Tachibana, T. Someya, and Y. Arakawa, Appl. Phys. Lett. **74**, 383 (1999).
[27] R. A. Oliver, G. A. D. Briggs, M. J. Kappers, C. J. Humphreys, S. Yasin, J. H. Rice, J. D. Smith, and R. A. Taylor, Appl. Phys. Lett. **83**, 755 (2003).
[28] D. P. Williams, A. D. Andreev, E. P. O'Reilly, J. H. Rice, J. W. Robinson, A. Jarjour, J. D. Smith, R. A. Taylor, G. A. D. Briggs, Y. Arakawa *et al.*, in *Physics of Semiconductors: 27th International Conference on Semiconductor Physics*, AIP Conf. Proc. No. 772, edited by José Menéndez and Chris G. Van de Walle (AIP, Melville, NY, 2005), p. 695.